INTEGRAL

Science Operations Centre

Announcement of Opportunity for Observing Proposals

JEM-X Observer's Manual

INTG-AO-00047

Issue 1.0

4 September 2023

Prepared by:

Celia Sánchez-Fernández

Based on inputs from the JEM-X team, National Space Institute, Technical University of Denmark (PI: S. Brandt); P. Kretschmar, ISOC, ESA/ESAC, Madrid, Spain, and E. Kuulkers, A. Orr, ESA/ESTEC, Noordwijk, The Netherlands.

Table of Contents

1 Introduction

The Joint European Monitor for X-rays (JEM-X) on-board INTEGRAL fulfils several roles. It provides complementary data at lower energies (3-35 keV) for the studies of the gamma-ray sources observed by the two main gamma-ray instruments, IBIS and SPI. Normally any gamma-ray source bright enough to be detected by the main instruments will also be bright enough to be rapidly identified with JEM-X. Flux changes or spectral variability at the lower energies may provide important elements for the interpretation of the gamma-ray data. In addition, JEM-X has a higher angular resolution than the gamma-ray instruments. This helps with the identification of sources in crowded fields.

JEM-X can also deliver independent scientific results concerning sources with soft spectra, such as the emergence of new transients or unusual activity in known sources, serendipitously detected in the FOV during the normal observations. Some of these sources may not even be detectable by the other instruments onboard INTEGRAL. Note, however, that the field of view (FOV) of JEM-X is significantly smaller than those of IBIS and SPI.

JEM-X operates simultaneously with IBIS and SPI. It is based on the same principle as the two gamma-ray instruments on INTEGRAL: sky imaging using a coded aperture mask. The performance of JEM-X is summarised in Table 1. In Figure 1 the total effective area of JEM-X is shown.

The following Sections give a description of the instrument (Section 2), its operations (Section 3), its performance (section 4), and hints on the use of the instrument (so-called "cook book"; Section 5). For more details, we refer the reader to a sequence of papers on the JEM-X payload in the A&A special INTEGRAL issue (2003, Vol. 411, L231-L256). This issue also contains various other papers on the first results from in-flight observations. For a description of the JEM-X data analysis refer to Westergaard et al. (2003, A&A 411, L257). The JEM-X validation report of the **O**ff-line **S**cientific **A**nalysis (OSA) software package released by the ISDC, as well as descriptions of the data analysis pipelines and modules and the use of the OSA software can be found at the ISDC website (http://www.isdc.unige.ch/integral/analysis).

Table 1: parameters and performance of the JEM-X1 unit

Parameter	**In-orbit value**
Active mask diameter	535 mm
Active detector diameter	250 mm
Distance from mask to detector entrance window	3401 mm
Energy range	3-35 keV
Energy resolution (FWHM)	$\Delta E/E = 0.40 \times [(1/E\ \text{keV})+(1/8\ \text{keV})]^{1/2}$
Angular resolution (FWHM)	3′
Field of view (diameter)	4.8° Fully illuminated 7.5° Half response* 13.2° Zero response
Relative point source location error	1′ (90% confidence radius for a 15σ isolated source)
Continuum sensitivity **for two JEM-X units combined** (isolated source on-axis)	8.5×10^{-5} ph cm^{-2} s^{-1}keV^{-1}@ 6 keV 7.1×10^{-5} ph cm^{-2} s^{-1}keV^{-1}@ 30 keV for a 3σ continuum detection in a 10^5 s observation with ΔE = 0.5E
Narrow line sensitivity **for two JEM-X units combined** (isolated source on-axis)	1.7×10^{-4} ph cm^{-2} s^{-1}@ 6 keV 1.3×10^{-4} ph cm^{-2} s^{-1}@ 20 keV for a 3σ line detection in a 10^5 s observation
Timing resolution	122 μs (relative timing) ≈1 ms (absolute timing)

* At this angle, the sensitivity is reduced by a factor 2 relative to the on-axis sensitivity. In practice, the transmission of the collimator beyond an off-axis angle of 5° is so low that only the very brightest sources can be observed at larger angles.

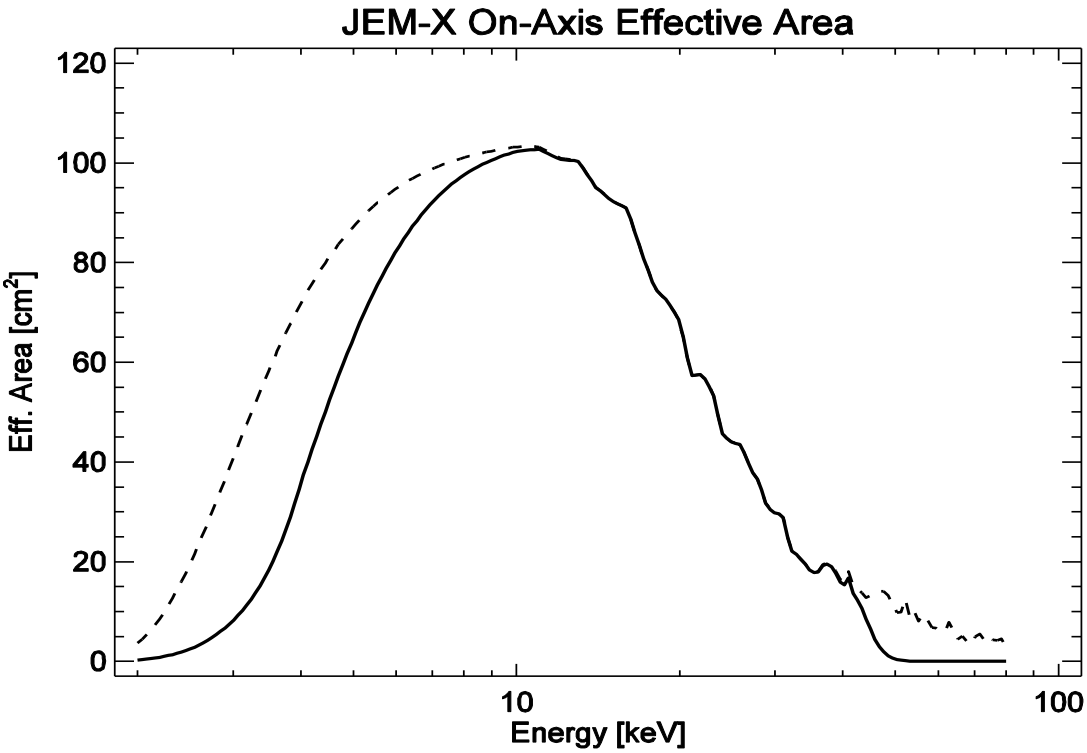

Figure 1: Total effective area of one JEM-X instrument. The dashed curve shows the area before electronic effects are taken into account. The full curve includes the rejection of low signals as well as very high signal

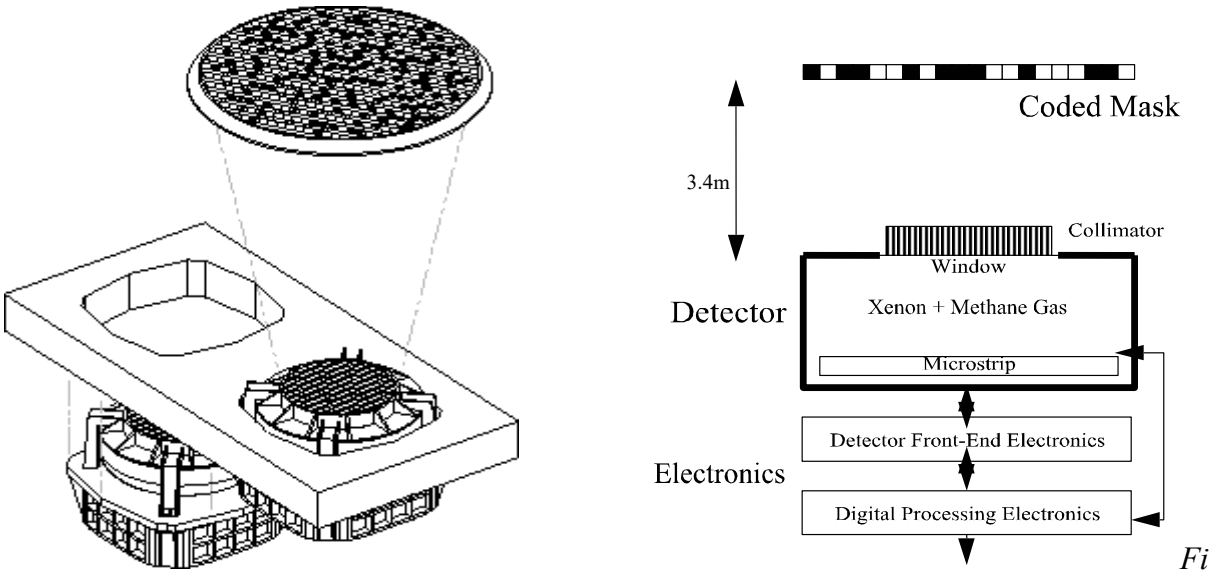

Figure 2: Left: overall design of JEM-X, showing the two units, with only one of the two coded masks. Right: functional diagram of one unit.

2 Description of the instrument

2.1 The overall design and status

JEM-X consists of two identical coded-aperture mask telescopes co-aligned with the other instruments on INTEGRAL. The photon detection system consists of high-pressure imaging Micro-strip Gas Chambers located at a distance of 3.4 m from each coded mask.

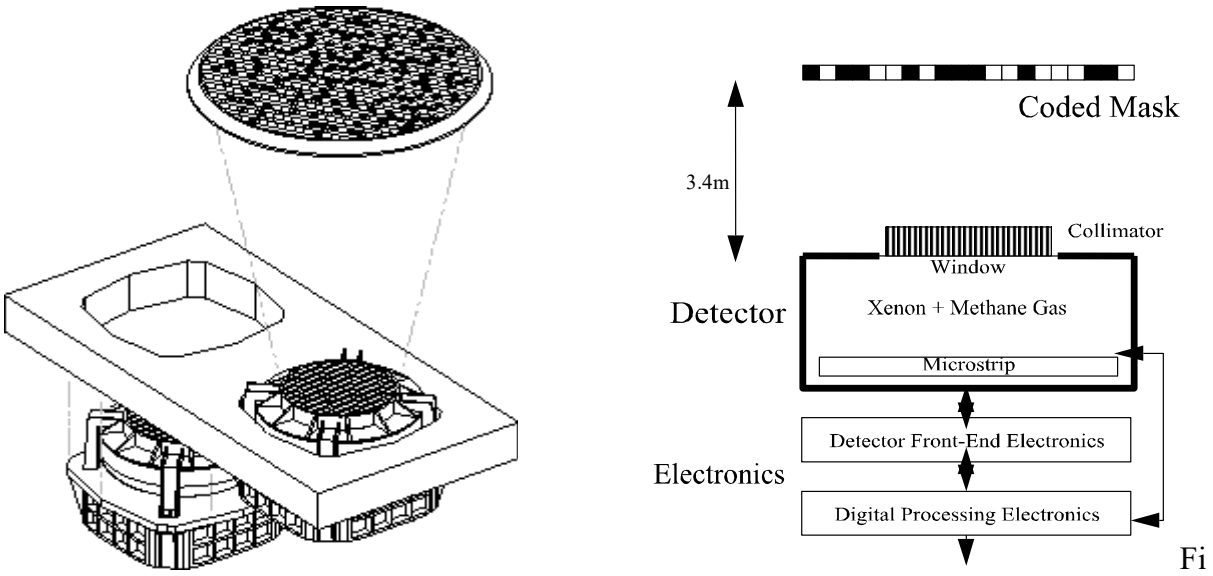

Figure 2 shows a schematic diagram of one JEM-X unit. A single JEM-X unit comprises three major subsystems: the detector, the associated electronics (see also Figure 6) and the coded mask. Since revolution 976 (Oct. 10, 2010) both JEM-X units are operating together.

The dead anodes with permanently low or no activity are taken into account in the OSA analysis software. The latest update on the number of dead anodes is from September 2021, and counts to 67 on each JEM-X.

The JEM-X detector is a micro-strip gas chamber with a sensitive geometric area of 500 cm^2 per unit. The filling gas is a mixture of xenon (90%) and methane (10%) at 1.5 bar pressure. The incoming photons are absorbed in the xenon gas by photo-electric absorption and the resulting ionisation cloud is then amplified in an "avalanche" of ionisations by the strong electric field near the micro-strip anodes. Significant electric charge is picked up on the strip as an electric impulse. The position of the electron avalanche in the direction perpendicular to the strip pattern is measured from the centroid of the avalanche charge. The orthogonal coordinate of an event is obtained from a set of electrodes deposited on the rear surface (backplane) of the plate.

Hotspots appear from time to time on the detector micro-strip plate. They are weak except at very low energies (<2.5 keV) where their peak intensity can be high (up to 100 cts/s), but they last only minutes, at most hours, not days. Their physical extent is a few mm^2. They are identified by the OSA analysis software in the data correction step and are consequently excluded from further analysis. So far, no "hot strips" have been detected

The X-ray window of the detector is composed of a thin (250 μm) beryllium foil which is impermeable to the detector gas but allows a good transmission of low-energy X-rays, down to the beryllium cutoff energy, starting at 2-3 keV.

A collimator structure with square-shaped cells is placed on top of the detector entrance window. It gives support to the window against the internal pressure and, at the same time, limits and defines the field of view of the detector. It has an 85% on-axis transparency. The collimator is important for reducing the count rate caused by the cosmic diffuse X-ray background. However, the presence of the collimator also means that sources near the edge of the field of view will be attenuated with respect to on-axis sources (see Figure 3). The materials for the collimator (molybdenum, copper, aluminium) have been selected in order to minimise the detector background caused by K fluorescence.

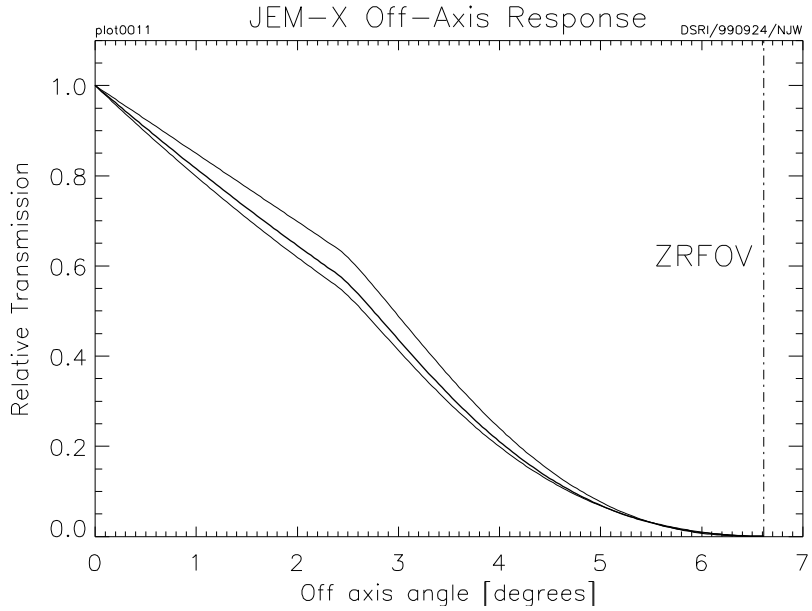

Figure 3: Off-axis response of JEM-X. The middle curve shows the average transmission through the collimator, including all azimuth angles.

Four radio-active sources are embedded in each detector collimator in order to calibrate the energy response of the JEM-X detectors in orbit. Each source illuminates a well defined spot on the micro-strip plate. JEM-X1 has two Cd-109 and two Fe-55 sources radiating at 22 keV and 5.9 keV, respectively. JEM-X2 has four calibration sources with Cd-109. The gain of the detector gas has

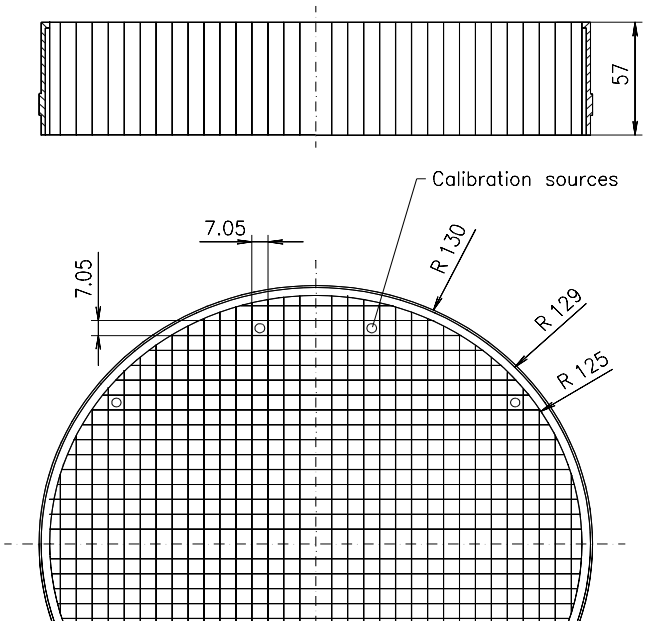

Figure 4: Collimator layout. In this diagram the 4 calibration sources are situated on the upper side. The dimensions are in mm, i.e., collimator height = 57 mm and radius = 130 mm.

been monitored continuously with the help of these sources. Since the beginning of the mission, the strength of the Cd sources has dropped by a factor of about 1400, while the Fe sources have declined by only a factor of 30. Consequently, since revolution 1498 (February 2015) both JEM-X units are calibrated using the two Fe sources in the JEM-X1 unit. This method has proven to give excellent results. Figure 4 shows the collimator layout and the locations of the calibration sources.

2.2 The coded mask

The mask is based on a Hexagonal Uniformly Redundant Array (HURA). For JEM-X, a pattern composed of 22501 elements with only 25% open area has been chosen. The 25% transparency mask actually achieves better sensitivity than a 50% mask.

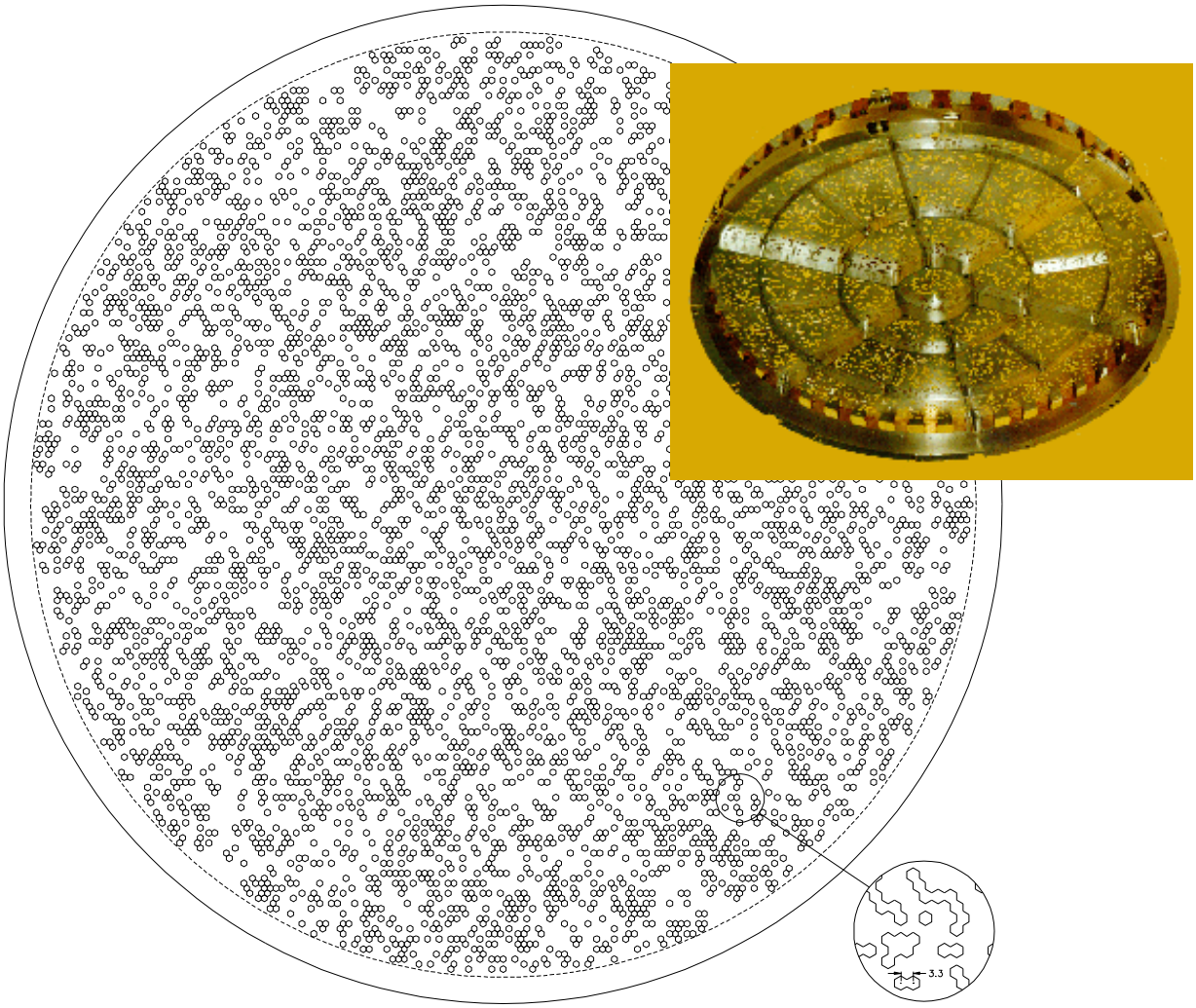

Figure 5: Illustration of the JEM-X coded mask pattern layout without the mechanical interface. The diameter of the coded mask is 535 mm. The mask has a transparency of 25%. A picture of the mask is shown at the top right.

The JEM-X imaging is affected by some (limited) coding noise, but does not suffer from "ghost" images, except in rare cases, because the pattern of the mask only repeats itself near the edges of the mask.

The mask height above the detector (3.4 m) and the hexagonal mask element dimension (3.3 mm centre-to-centre) define together the angular resolution of the instrument. *Figure 5* illustrates the JEM-X coded mask pattern.

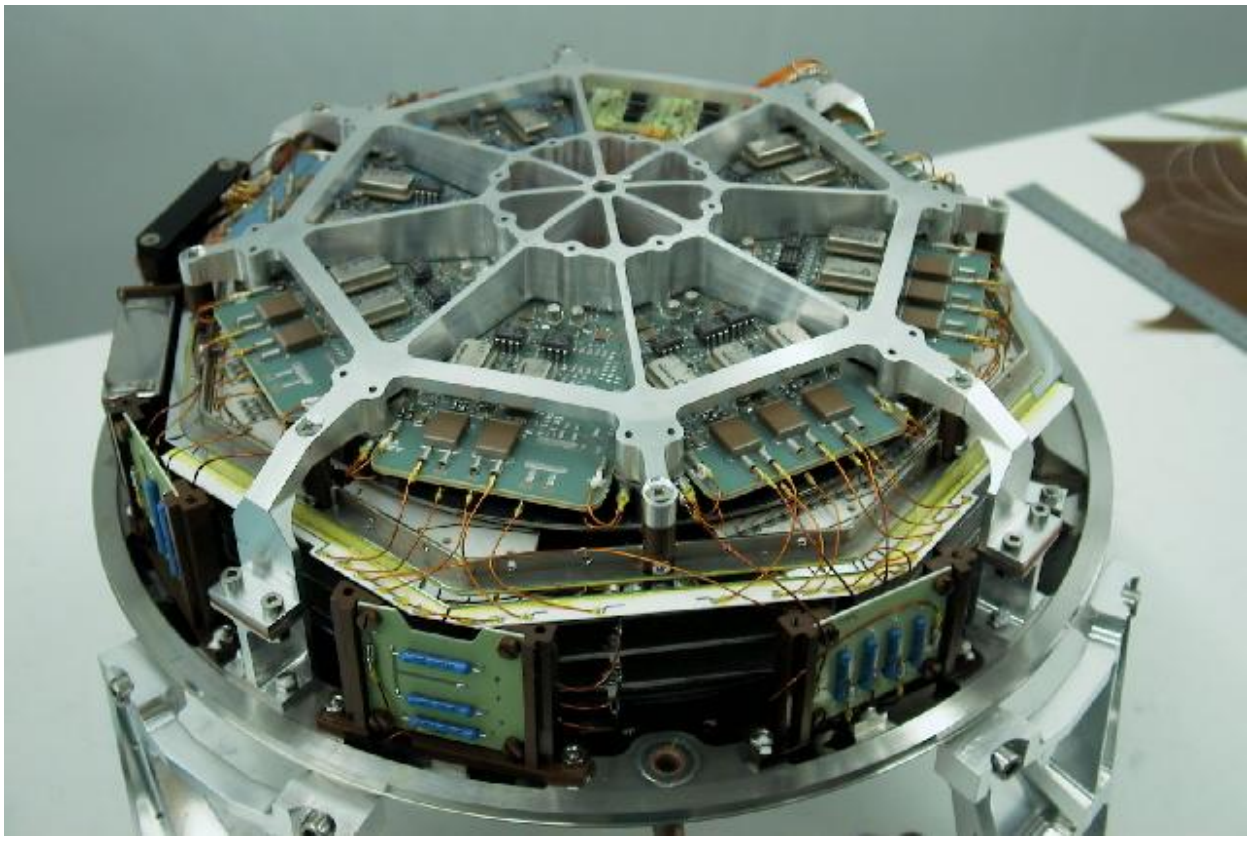

Figure 6: JEM-X Qualification Model detector during assembly.

3 Instrument operations

3.1 Telemetry formats and their use

In order to make the best of a situation with a limited telemetry band-width, two types of on-board data reduction can in principle take place for the JEM-X instruments:

1) A grey filter can randomly remove *some of the events* from the telemetry data stream. This takes place automatically when the telemetry buffer fills up beyond a certain limit and will typically happen for JEM-X count rates higher than about 150 counts/s including background, or about 1 Crab, at standard telemetry allocation.

2) The on-board software can switch to a "reduced event" telemetry format which removes *part of the information* about each event from the telemetry data stream. For each observation, two formats, "primary" and "secondary" can be defined. Observations will begin in the "primary" format and can switch to the "secondary", if the current count rate is too high – and switch back again if the possibly higher transmission rate is no longer required.

In practice, all data formats except for the "Full Imaging" default format suffer various shortcomings – e.g., lack of spatial gain corrections due to the lack of positional data or very limited support within the OSA software – that make them of little use to general observers. Therefore, the telemetry format can not be chosen by the user in the Proposal Generation Tool (PGT), but is pre-set to "Full Imaging" for primary and secondary format on-board.

In the unlikely case that a specific observation requires the use of another telemetry format than "Full Imaging", the observer needs to specify and justify this fact in the scientific justification. If the proposal is accepted, ISOC would then set the required modes before scheduling the proposal.

3.2 The grey-filter mechanism

The grey-filter process can operate with 32 different transmission fractions. These fractions are 1/32, 2/32, …, 31/32, 32/32. The filter values to be used will be chosen by the instrument electronics during the actual observation, taking into account the total background count rates. The grey filter will always be adjusted automatically by the on-board software to match the data stream to the available telemetry capacity, thus the term "automatic grey filter". Whenever the grey filter level is changed (decreased or increased) the on-board software checks whether a telemetry format change should also take place – in the default set-up (see above), this has no effect, as the "Full Imaging" format is used throughout.

Users should be aware that during periods of heavy grey filtering (strong sources in the FOV) the energy determination will be worsened due to a lack of calibration photons. Usually the energy correction can be determined to within 1-2%, but grey filtering may broaden this value to 4-5%.

3.3 TM buffer flushing

The JEM-X instruments have an internal buffer capable of storing up to 60,000 events. This allows JEM-X to accommodate temporary count rate increases without data loss. But if the telemetry allocation averaged over a science window does not allow transmission of all events, then those events which remain in the on-board buffer when a new observation starts, will be flushed and lost.

3.4 Detailed overview of the telemetry formats

The following information is given for reference only, as the "Full Imaging" format is the only format that has been calibrated and is fully supported by the OSA analysis software.

Table 2: Characteristics of the JEM-X Telemetry Format.

Format Name	Detector Image Resolution (pixels)	Timing Resolution	Number of Spectral Channels	Event rate (cps) until onset of grey filter
Full Imaging	**256 x 256**	**1/8192s = 122μs**	**256**	**70**

4 Performance of the instrument

JEM-X currently operates with both units active. The nominal telemetry allocation is 12 science packets and 1 housekeeping packet per 8 seconds for each unit. This allows transmission of about 150 counts/s before events begin to pile up in the onboard buffer – this will eventually force the grey filter mechanism to set in (150 counts/s corresponds to about the count rate for a ~1.2 Crab source plus the solar minimum instrumental background). At the beginning of a new pointing ("science window") the grey filter is set to full transmission, and therefore, even for higher count rates there will always be a period in the beginning of every pointing where all data are transmitted – the catch is that some of the data taken at the end of the pointing may be lost as the onboard buffers are flushed when the following pointing begins.

4.1 Background

The JEM-X background during solar minimum conditions has been measured from a number of empty field observations. The background rate is about 40 counts/s in the 3 to 35 keV range, when the spacecraft is outside the radiation belts. Figure 7 shows a background spectrum from JEM-X 2, averaged over 46 science windows in August 2008 (revolution 716).

The background radiation environment is mainly produced by two components: the diffuse X-ray background and the X- and gamma-radiation induced by cosmic rays. The diffuse X-ray background dominates the background below about 15 keV and the cosmic ray induced background dominates at higher energies. The line at about 30 keV is due to fluorescence photons from the Xenon gas in the volumes surrounding the active detector volume. It is now an essential calibration line and an indicator of the effective resolution of the instrument.

There are other instrumental lines visible as well. The background increases noticeably at the edge of the detector which is why the useful detector diameter is only 220 mm, rather than the 250 mm physical diameter. The useful diameter depends on the chosen energy range because the background distribution is strongly energy dependent. The rejection of background events produced by charged particles crossing the detector is accomplished with a combination of pulse height, pulse shape and "footprint"-evaluation techniques. These techniques achieve a particle rejection efficiency better than 99.5%.

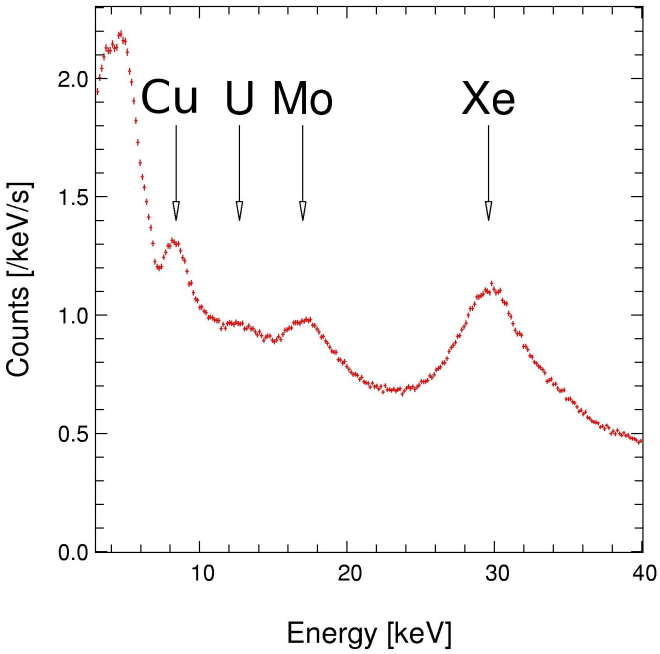

Figure 7: Full JEM-X 2 detector spectrum of empty field observations with diffuse and instrumental background. The most significant fluorescent lines are indicated (the uranium is from contamination in the Be-window).

4.2 Timing stability and resolution; dead-time

JEM-X observations of the Crab pulsar have shown that the absolute timing is stable to better than 100 μs. The individual JEM-X counts are binned into time bins with a width of 122 μs. However, the Crab analysis shows that the phase of the timing bins is stable within a few μs.

The dead-time depends on the total event trigger rate which is dominated by the particle background, and on the telemetry format used (exclusively 'FULL' with rare exceptions). In the current particle background condition, the dead-time fraction amounts to about 18%.

4.3 Detector energy resolution

The energy resolution of the JEM-X instruments slowly degrades with time when the instruments are used. This was one important reason why only one JEM-X unit was used at a time until revolution 975 (see Section 2.1). Three effects have been observed to change over time: one is an increase in the recovery time for local modifications (drops) in the gas amplification following large charge deposits on the micro-strip plate caused by the passage of heavy cosmic rays (glitches). The second effect is a gradual increase of the gas amplification for a constant detector voltage. This change is not the same everywhere on the detector, and requires remapping the gain map variation using the xenon fluorescence line from time to time. Physically, the degradation is suspected to be caused by gradual changes in the conductivity of the micro-strip glass substrate due to ion migration. The last aging effect is a significant increase

in the instruments' gain variation with temperature. Again, the size of this increase varies across the microstrip plates. The JEM-X instrument team generates offline a new Gain History table for every revolution to ensure the best possible gain determination despite the changing properties of each detector. Users should set up their systems to automatically receive updates of the ISDC IC tree that contains these tables. The JEM-X team generates regular updates to the response files to be used with the OSA, in order to take into account this evolution.

The degradation of the energy resolution is most noticeable at the highest energies. It can be described by an additional, slowly time-varying, term in the following equation:

$$\Delta E/E = 0.4 \times [(1 / E\ [keV]) + (1 / E_{noise}\ [keV])]^{1/2}.$$

E_{noise} can be interpreted as the energy where the resolution has degraded by a factor $\sqrt{2}$. For JEM-X2, E_{noise} is close to 8 keV. While the current detector energy resolution is around 20% and continues to degrade for the various reasons stated above. The determination of line centroids can still be found to about 2% accuracy for most SCWs, though this is degraded to about 4-5% for strong sources with heavy grey filtering.

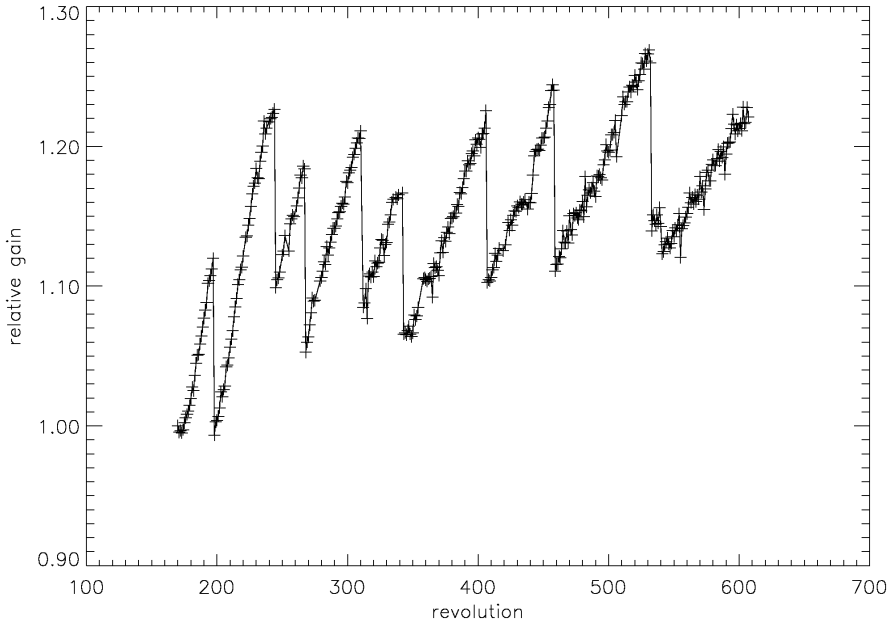

Figure 8: Average gain per orbit for JEM-X1 normalized to the gain of revolution 170. The average has been adjusted for a temperature dependent gain variation to show the overall trend of gain increase over time. The steps in gain correspond to the lowering of the high voltage setting. A similar development is found for JEM-X2 where the cathode voltage is adjusted so that the gain remains constant within +/-10% (disregarding temperature effects that may add or subtract about 5%). The effect of the changing gain has been significantly improved in the successive OSA software releases.

4.4 Detector gain

There are four radio-active calibration sources in each of the JEM-X detectors. JEM-X1 has two Cd-109 and two Fe-55 sources radiating at 22 keV and 5.9 keV, respectively. JEM-X2 has four calibration sources with Cd-109. The detector gain is monitored continuously by the counts from these sources. Since revolution 1498 only the Fe calibration sources in the JEM-X unit have been used for energy determination. The Cd-109 sources are far too weak and would only add noise and increased uncertainty to the energy corrections. The gain of the JEM-X detectors has been found to increase slowly over time. By lowering the high voltage at suitable times the gain is confined to a limited band (see Figure 8). On top of this, the gain is also dependent on the detector temperature (currently about 5% change per ºC, and still increasing), but all of this is automatically corrected for in the analysis correction level, which uses instrument characteristics tables created one per instrument per revolution since revolution 949, and for some revolutions previous to this. See JEM-X analysis manual for details.

A full archive of JEM-X gain and energy determination characteristics can be seen at: http://spacecenter.dk/~oxborrow/sdast/GAINresults.html.

A similar archive of JEM-X HK values, temperature and event count rates can be found at: http://spacecenter.dk/~sb/JEMX/HK.htm.

4.5 Spectral analysis

For bright sources, spectra can be extracted in a straightforward manner using the spectrum extraction step of the OSA software. An example is given below in Figure 9 for the Crab. This gets more problematic for weak sources in crowded fields, where contamination from the brighter sources affects results. In these cases, extracting spectra from mosaic images is recommended. An example is given in Figure 10 for IGR J17254-325, a source of ~2 mCrab in the 3-10 keV band, surrounded by brighter sources. For more detailed information about the extraction of spectra, we refer to the ISDC's JEM-X User Analysis Manual available from http://www.isdc.unige.ch/integral/analysis.

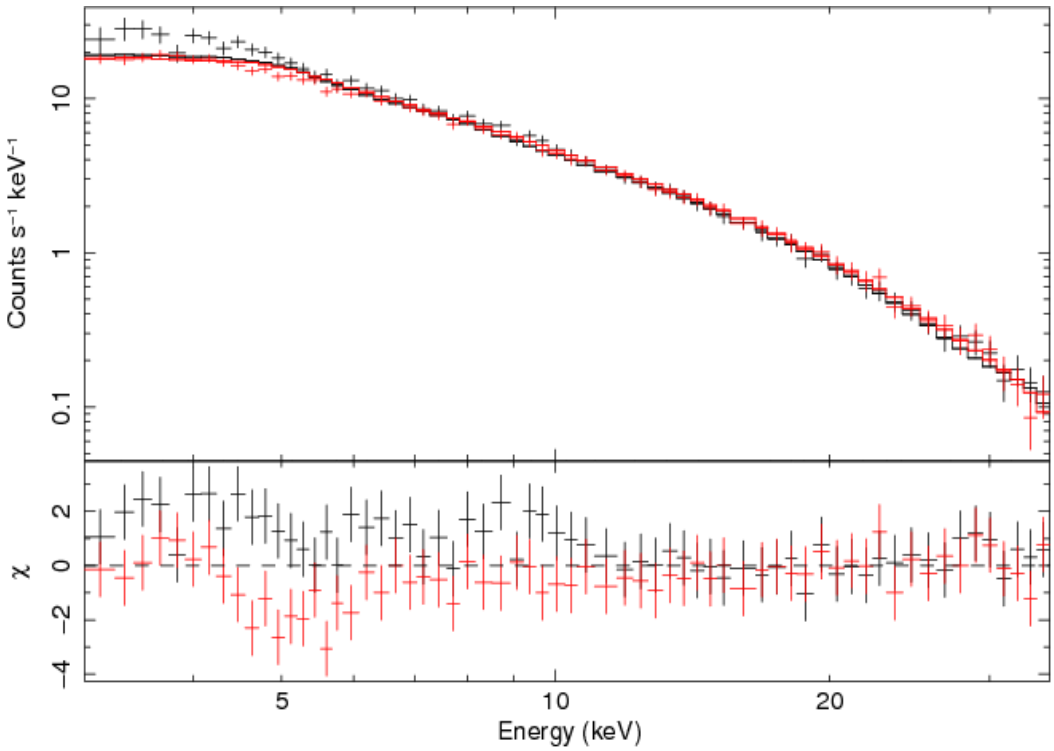

Figure 11: JEM-X1 (black) and JEM-X2 (red) Crab count spectra together with the simultaneous fit to a power-law emission model, $dN/dE=N(E/1\ keV)^{-\Gamma}$ ph cm^{-2} s^{-1} keV^{-1}, subjected to photo-electric absorption of $0.36x10^{22}$ atoms cm^{-2}, with $N=6.65$ ph cm^{-2} s^{-1} keV^{-1} and $\Gamma = 2.0$. The data are from revolution 39 with a total exposure time of 1.2 ksec. A systematic error of 3% has been added. The goodness-of-fit is $\chi^2=149$ for 126 degrees of freedom.

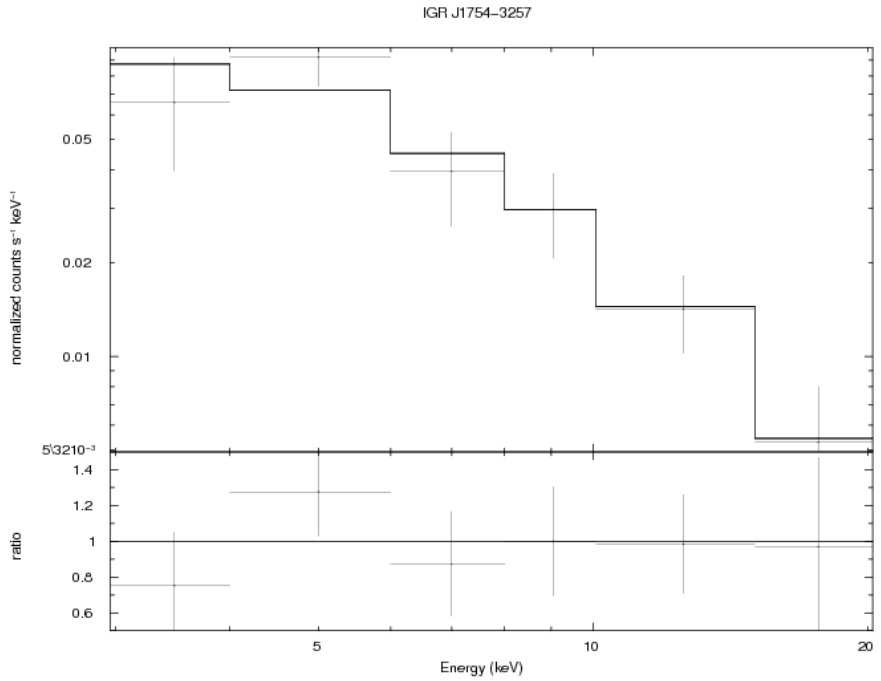

Figure 12: JEM-X spectrum of IGR J17254-3257, obtained from mosaic images with a total exposure time of ~310 ksec. The spectral fit shown is a simple power law.

4.6 X-ray burst detection

X-ray bursts can be searched for using JEM-X detector light curves with typically ~10 s time bins. In order to verify that a burst found in the detector light curve really comes from a point source, an image must be generated with an exposure time corresponding to the time interval of the burst, and then compared with a corresponding image covering an equivalent interval before or after the burst. Once the point source origin has been verified, the source light curve and spectrum can be extracted and investigated for the burst characteristics. As an example, we use the detection with JEM-X of the first observed X-ray burst from the source IGR J17254-3257 on February 17th, 2004 (Brandt et al. 2006, ATel #778).

shows the detector light curve (in black) together with source light curve of IGR J17254-3257 (in red) both in the 3-10 keV energy band, with 10 s time bins in a 6 minute time interval. One can actually see on the detector light curve another, stronger, burst from the source 1A 1742-294 occurring less than one minute after the former. The source light curve, which is vignetting corrected, shows that the IGR J17254-3257 burst peak is much more pronounced than in the raw detector light curve.

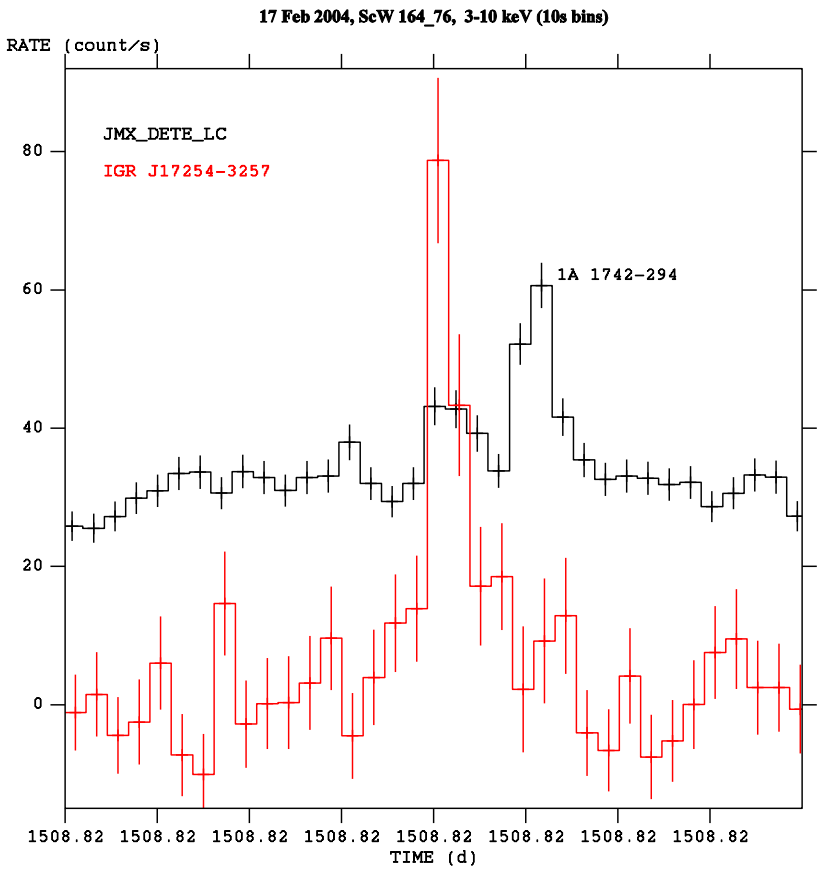

Figure 13: JEM-X detector light curve (black) and IGR J17254-3257 source light curve (red) during a 6 minute interval around the burst that occurred at UTC 19:44:00 on 17 February 2004. Note that another, stronger, burst from 1A 1742-294 occurred less than one minute after the event from IGR J17254-3257.

Figure 14 shows the 45 s exposure taken during the burst (left) where only IGR J17254-3257 is visible and the whole science window exposure (right) where a number of other sources are also visible, but not IGR J17254-3257, due to its very low persistent emission. A zoom around the position of IGR J17254-3257 is also displayed in each case.

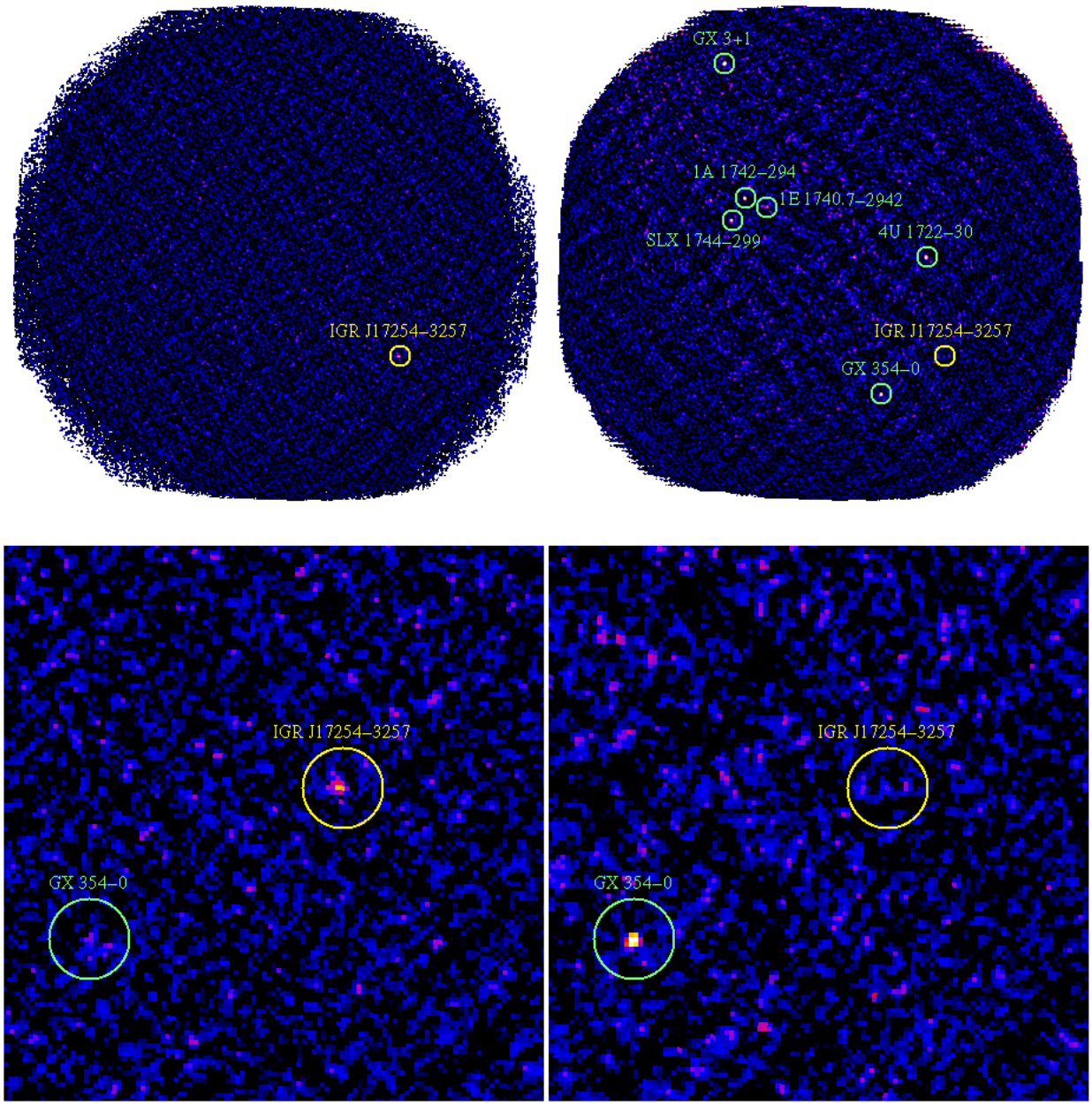

Figure 14: JEM-X 3-10 keV images obtained during a 45 s exposure around the X-ray burst from IGR J17254-3257 (left) and over the whole science window (right).

5 Observation "cook book"

5.1 Considerations of the use of the instrument

The primary role of JEM-X is to provide simultaneous data on the X-ray flux and variability of the targets observed by the two main gamma-ray instruments IBIS and SPI. JEM-X can often pinpoint the source positions with better precision than 2 arc minutes and is thus capable of contributing to the identification of new sources.

Users should also be aware that the current spectral extraction and vignetting corrections for sources with off-axis angles greater than 3 or 4 degrees should be interpreted with caution.

Concerning source detectability, it can be noted that during exposures of typically 2000s, practice has shown that sources down to about 6 mCrab and 3 mCrab (between 3-10 keV and 10-25 keV, respectively) are detected with a significance of 5σ if they are within the central few degrees of the field of view, and there are no other sources in the field of view contributing to the instrument background. These numbers refer to observations with a single JEM-X unit. When combining the two units these numbers change to about 5 and 2 mCrab.

5.2 Loss of JEM-X sensitivity due to 5x5 dithering

Most INTEGRAL observations are done using a 5x5 dither pattern with points spaced 2.17 degrees apart. Dithering is necessary for SPI and recommended for IBIS. Unfortunately, such dithering does not allow JEM-X to observe the target source continuously. In the 5x5 mode, only the central 9 out of the 25 dither pointings yield useful JEM-X spectral data for the central source. The target is simply too far off-axis during the remaining 16 dither pointings (see also Figure 3, page 9). Table 5 shows the average degradation for the different spacecraft dithering patterns. When JEM-X coverage is an essential part of the observation, the hexagonal dither pattern may be selected ("staring" is not recommended).

To further reduce systematic effects in deep mosaic images of IBIS/ISGRI, an offset between the centre of each dither (either 5x5 or hexagonal) cycle was introduced in AO3 for observations requiring several dithering cycles. This ensures that no pointing attitude is repeated over the course of the observation. Hence, the **C**entre **O**f a dither **P**attern (COP) moves around in a defined order during an observation (see the document ***Overview, Policies and Procedures***). With the COP move, the imaging noise in the JEM-X mosaic images has also been reduced. Additionally, a sequential rotation covering the range +/-3 degrees between successive repetitions of the same (5x5) pattern has been implemented by ISOC in AO5 (see again ***Overview, Policies and Procedures***).

Table 3: Effective JEM-X observation times for different dithering modes.

Dithering mode	Effective observation time
Staring	100%
Hexagonal dither	69%
''5 × 5'' dither	23%

5.3 How to estimate observing times

This section describes how to estimate observing times in order to detect X-ray continuum emission and line emission with JEM-X. It is assumed that there is *no dithering* (i.e. "staring" mode) and that only **one** JEM-X unit is used. The instrument sensitivities quoted here are basically the same as in previous AO's.

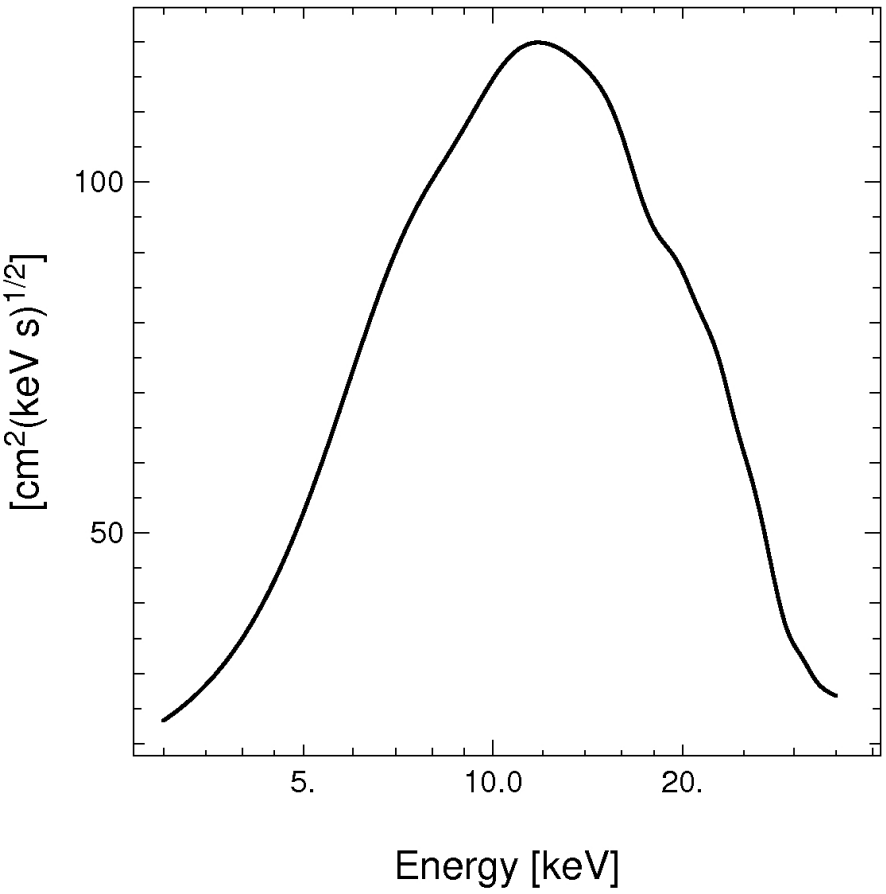

Figure 15: C-factor for estimating the continuum sensitivity for the combined JEM-X units for an on-axis source (see formula in Section 5.4).

5.4 Continuum emission

An estimate of the continuum sensitivity is obtained by the following expression:

$$N_\sigma = F_{cont}(E) \times \sqrt{\Delta E \times t_{obs}} \times C(E) \times \eta ,$$

where N_σ is the detection significance, $F_{cont}(E)$ is the continuum flux (in photons cm^{-2} s^{-1} keV^{-1}), t_{obs} is the exposure time (in seconds), ΔE is the width of the energy interval (in keV), and η is the vignetting factor for an off-axis source (see Figure 3). The factor 'C' depends on the detector properties and the background level. It can be obtained from Figure 15.

5.5 Imaging: resolution and detection limits

The accuracy of source position determinations depends on the number of sources, background counts and on the off-axis angle of the source. Analysis of the standard JEM-X images show that the point spread function of JEM-X is well represented by a symmetrical 2D Gaussian function, with a standard deviation of 1.2'. This resolution defines the ability to check for the presence of multiple sources, and also to separate spectra from two sources at small angular separations. The source positions are best determined when sources are observed on-axis. The JEM-X vignetting function has the shape of a pyramid, so even within the central "fully illuminated" region the instrument response varies significantly between different off axis positions.

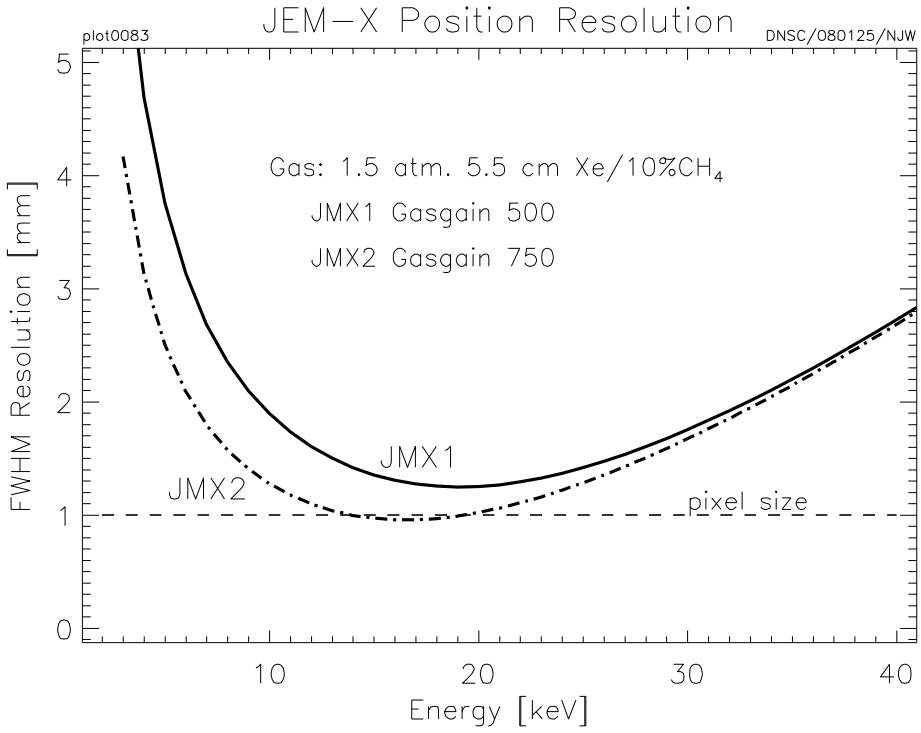

Figure 16: The positional resolution in the JEM-X1 and JEM-X2 detectors as a function of energy. Note that the positions are rounded to 1 mm accuracy in the down-linked data.

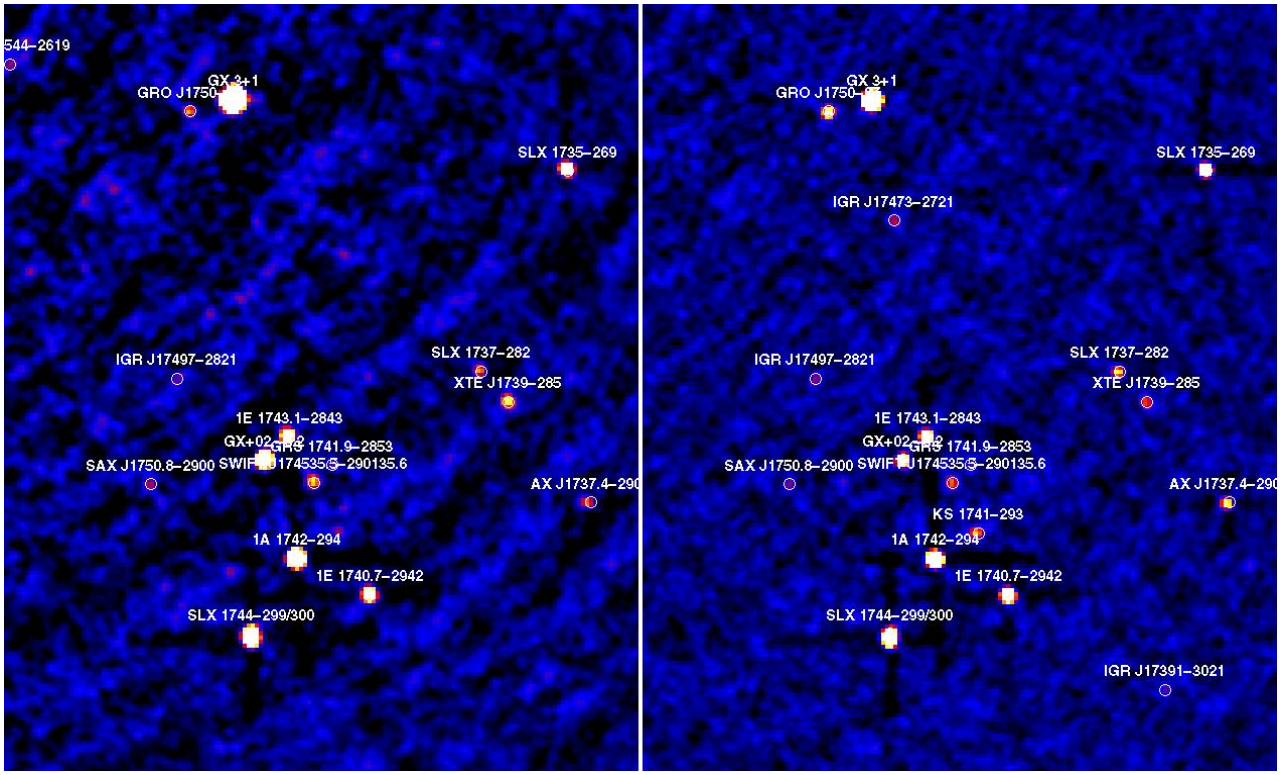

Figure 17: Deep mosaic significance image of the region around the Galactic bulge, based on over 3000 JEM-X exposures (science windows) in the 3-10 keV (left) and 10-25 keV (right) energy bands. The effective exposure at the centre is close to 3 Msec; the field is about 4°x5° wide.

The intrinsic detector position resolution is shown as function of energy in Figure 18 for photons entering on-axis. The degradation below 10 keV is caused by the electronic noise of the front-end amplifiers; above 10 keV it is caused by the increase of the primary photo-electron range with energy. The intrinsic positional resolution of the detector is finer than the pixel size of the coded mask (3.3 mm) over most of the energy range. The determination of the photon positions in the image plane is affected by parallax for higher energy photons entering at off-axis angles. This effect is not of prime importance for source positioning, but the smearing of the image affects the off-axis sensitivity at energies above 20 keV.

The alignment of the detector with respect to the INTEGRAL star tracker appears to be stable to better than 5" and the star tracker accuracy is even better than this. The JEM-X OSA software yields source positions to better than 10" provided the detection significance is high.

The source detection limit for single science windows also depends on the background conditions and on the off-axis angle of the source. However, sources as low as 10 mCrab are reliably detected under normal background conditions if they appear at less than 3˚ off-axis. Better sensitivities can be obtained by "mosaicking" overlapping images from several science windows. A deep mosaic image example is shown in Figure 19, while Figure 20 and Figure 19 illustrate the source detection capabilities obtained from mosaic images as a function of effective accumulated observation time (corrected for dead time, grey filter and vignetting effects).

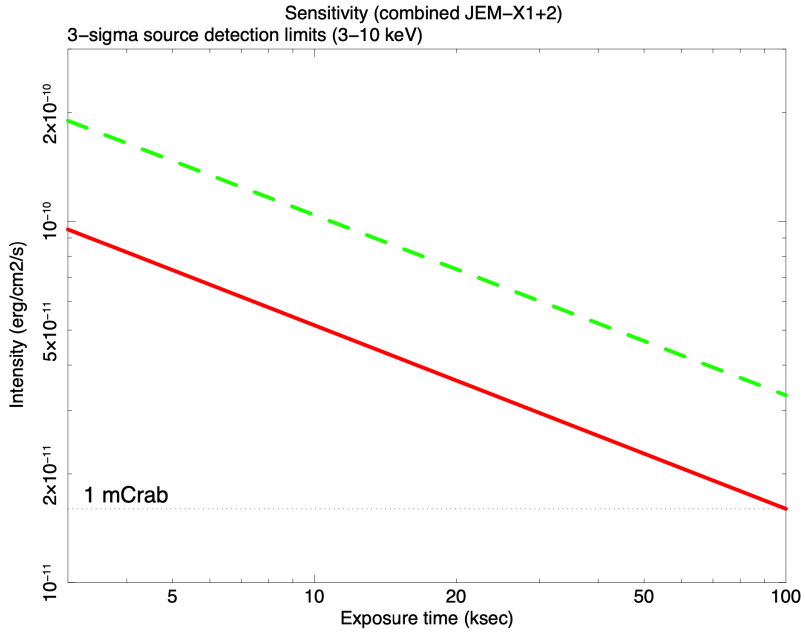

Figure 21: Source detection capabilities in the 3-10 keV energy band as a function of the accumulated effective exposure time in JEM-X mosaic images, corrected for dead time, grey filter and vignetting effects. The slope of the lines is obtained from simulations where an isolated source must be detected at 3σ in the deconvolved image. The dashed line represents the case where there are additional sources in the field of view giving a background corresponding to a total of 1 Crab. The positions of the lines are determined by actual measurements.

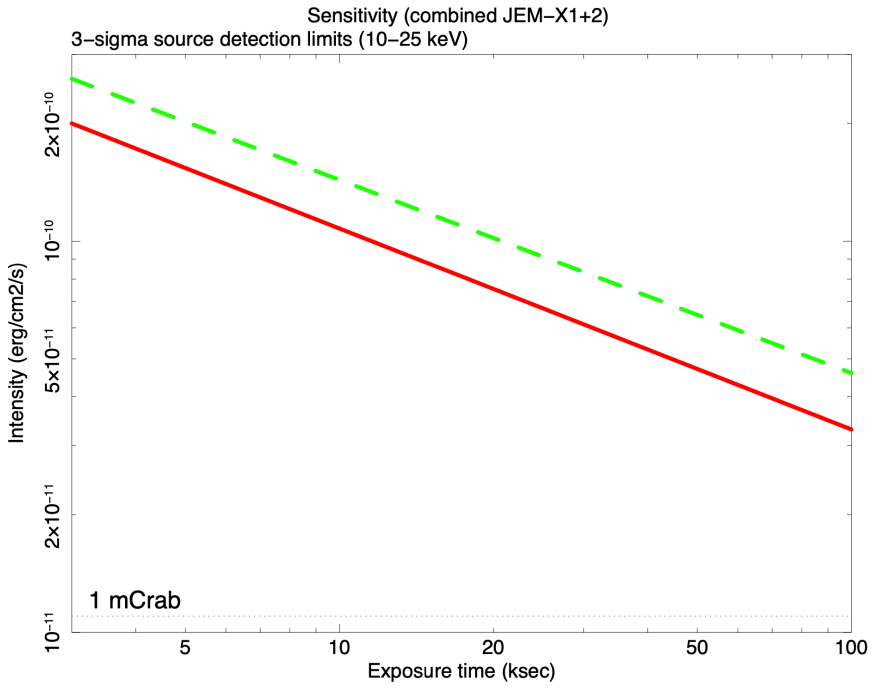

Figure 19: Same as Figure 22 but for the energy range from 10 to 25 keV.

JEM-X's good spatial resolution also makes it possible to analyse extended sources. An example is the Ophiuchus cluster, which is bright in the X-ray region. A JEM-X significance image is shown in Figure 20. Clearly, the cluster emission is extended; the angular size of the X-ray source at half-maximum is 3.2', and therefore the morphology can be investigated.

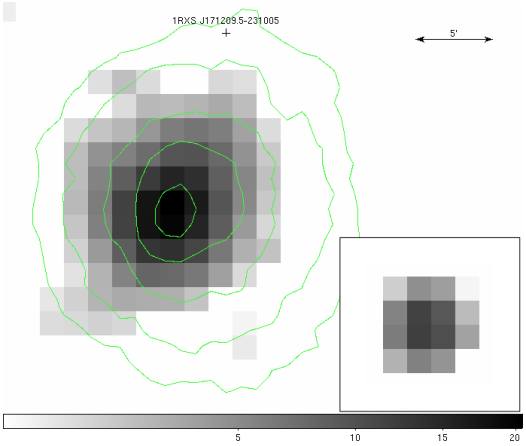

Figure 20: JEM-X significance image of the Ophiuchus cluster in the 3-18 KeV band, with the surface brightness contours from ASCA overlayed. The inset shows the image of a known point source (V2400 Oph, a cataclysmic variable) in the same field, demonstrating the extended nature of the cluster. The cross shows the position of 1RXS J171209.5-231005, the nearest known X-ray point source. (From Eckert et al. 2008, A&A 479, 27)

An imaging technique (PIF-imaging) has been developed, which improves the visibility of weak sources close to strong sources in the JEM-X images and mosaics. In images produced using *j_ima_iros* the image noise increases significantly around strong sources like, for example, GRS 1915+105 or when imaging the Galactic bulge. The PIF-imaging technique suppresses this effect. The method is based on a weighted back-projection of the detector pixels, where the weights depend on the illumination of each pixel by strong sources – i.e. sources detected by the source finding section of *j_ima_iros*. The image quality improvement is illustrated in Figure 21.

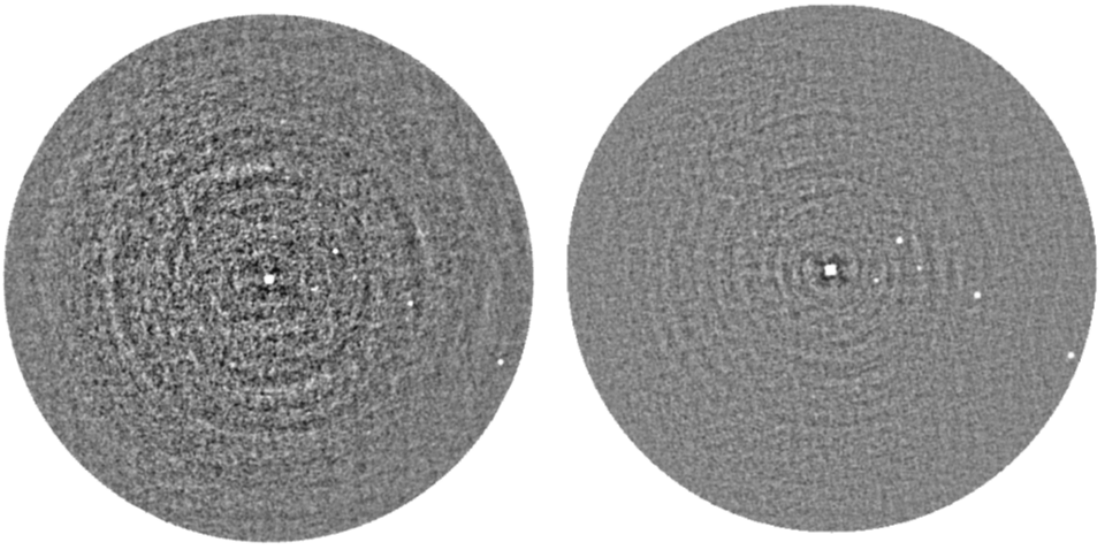

Mosaic from conventional images Mosaic from PIF-images

Figure 21: Comparison of a mosaic image around GRS 1915+105 produced by j_ima_iros (left) and the PIF_imaging technique

5.6 Practical examples

This Section gives some practical examples which illustrate the use of the formula described in the previous section. To conclude, Table 4 lists the actual JEM-X background count rates for a single JEM-X unit. The observed count rates for the Crab (Nebula and pulsar) on-axis, as measured in-orbit are provided in Table 5 and 6.

Table 4: Background count rates for a single JEM-X unit.[†]

Interval [keV]	**Diffuse X-ray Background counts s^{-1}**	**Cosmic Ray induced counts s^{-1}**	**Total bkg counts s^{-1}**
3 - 10	2.7	5.0	7.7
10 - 20	1.7	5.4	7.1
20 - 35	0.5	8.5	8.9
Total: 3 - 35	4.9	18.8	23.7

Table 5: JEM-X1 and JEM-X2 averaged Crab Count Rates extracted from on-axis ScWs 262700300010, 262700300020, and 262700300030 using different approaches.

	Images		Lightcurves		Spectra	
Energy range	**JMX1**	**JMX2**	**JMX1**	**JMX2**	**JMX1**	**JMX2**
3 - 10 keV	113 ± 1	96 ± 1	119.5 ± 8	109 ± 8	106 ± 1.4	88 ± 1.4
10 - 20 keV	29 ± 0.5	26 ± 0.4	22.5 ± 3	23 ± 3	24 ± 0.8	22 ± 0.8
20 - 33.5 keV	4.5 ± 0.2	4.5 ± 0.2	4.4 ± 2	5.2 ± 2	5.2 ± 0.4	5.2 ± 0.4
3 - 35 keV	138 ± 1	111 ± 1	148 ± 10	135 ± 8	140 ± 2	121 ± -2

[†] The observed source count rates given here are obtained from a spectral extraction and are only indicative, as they may change a few percent from observation to observation. The observed count rates do also depend on the extraction method, and one can for instance not expect to obtain the same measures directly from the images by e.g. 'mosaic_spec'.

Table 6: Same as Table 5, but for both JEM-X units combined [(JMX1+JMX2)/2].

Energy range	Images	Light curves	Spectra
3 - 10 keV	105 ± 1.4	114 ± 11	97 ± 2
10 - 20 keV	28 ± 0.6	23 ± 4	23 ± 1
20 - 35 keV	4.5 ± 0.9	5.2 ± 3	5.2 ± 0.6
3 - 35 keV	125 ± 1.4	142 ± 13	130 ± 3

5.6.1 Continuum studies

Consider a 10 mCrab (3-10 keV)‡ AGN with a photon spectral index of 1.7. How much observation time is needed for a continuum detection at various energies?

Assume a staring on-axis observation, i.e., with no sensitivity loss due to dithering and no other strong sources in the field of view. We can then estimate the time needed to get a 5σ detection in a prescribed energy band. Table 7 shows the result at three selected energies and energy bands.

Table 7: JEM-X continuum sensitivity study

E(keV)	ΔE(keV)	Flux (photons $cm^{-2}s^{-1}keV^{-1}$)	C(E)	Required Exposure Time (s)
4	2	4.6×10^{-3}	35	670
10	4	9.7×10^{-4}	116	700
20	6	3.0×10^{-4}	88	8500

5.6.2 Comparing 5x5 dither and hexagonal dither

The usual observation mode of INTEGRAL involves shifting the boresight in a dither pattern, most often a 5x5 pattern with a step size of 2.17 degrees. A hexagonal pattern (7 pointings) with an offset of 2 degrees is also an option.

Given a total observation time and a source in the center of the dither pattern, the detection significance, N_σ (formula in Section 5.4), for JEM-X will be about twice as large for the hexagonal pattern as for the 5x5 pattern, where in 64% of the time the off-axis angle is larger than 4 degrees.

‡ The somewhat ill-defined unit is here taken to use the source flux integrated over the energy interval from 3 to 10 keV relative to the Crab flux integrated over the same interval.